

Femtosecond Dynamics of the *tert*-Butyl Radical, *t*-C₄H₉

Bastian Noller,[†] Raman Maksimenka,[†] Ingo Fischer,^{*,†} Mario Armone,[‡] Bernd Engels,[‡] Christian Alcaraz,[§] Lionel Poisson,^{*,||} and Jean-Michel Mestdagh^{||}

University of Würzburg, Institutes of Physical and Organic Chemistry, Am Hubland, D-97074 Würzburg, Germany, Laboratoire de Chimie-Physique, Université Paris-Sud, Bât 349, F-91405 Orsay Cedex, France, and Laboratoire Francis Perrin, CEA/DSM/DRECAM/SPAM–CNRS URA 2453, DSM CEA Saclay, F-91191 Gif-sur-Yvette Cedex, France

Received: September 18, 2006; In Final Form: December 30, 2006

The excited-state dynamics of the *tert*-butyl radical, *t*-C₄H₉, was investigated by femtosecond time-resolved photoionization and photoelectron spectroscopy. The experiments were supported by ab initio calculations. *tert*-Butyl radicals, generated by flash pyrolysis of azo-*tert*-butane, were excited into the A ²A₁ (3s) state between 347 and 307 nm and the 3p band at 274 and 268 nm and ionized by 810-nm radiation, in a [1 + 2'] or [1 + 3'] process. Electronic structure calculations confirm that the two states are of s and p Rydberg characters, respectively. The carbon framework becomes planar and thus ion-like in both states. The photoelectron spectra are broad and seem to be mediated by accidental intermediate resonances in the probe step. All time-resolved photoelectron spectra can be described by a single decay time. For the A ²A₁ state, lifetimes between 180 and 69 fs were measured. Surprisingly, a much longer lifetime of around 2 ps was found for the 3p state. To understand the decay dynamics, the potential energy was computed as a function of several important nuclear coordinates. A [1,2] H-atom shift to the isobutyl radical seems not to be important for the excited-state dynamics. Qualitative considerations indicate curve crossings between the ground state, the 3s state, and a valence state along the asymmetric C–C stretch coordinate that correlates to the dimethylcarbene + methyl product channel. The implications of the present study for earlier work on the nanosecond time scale are discussed.

Introduction

Considerable effort is dedicated to understanding the reaction dynamics of alkyl radicals, because of their importance as reactive intermediates in combustion chemistry and hydrocarbon cracking¹ but also in the chemistry of planetary atmospheres.^{2,3} Despite the great interest in radicals, only little information is available in this area because of the experimental challenge. In particular, the excited-state structure and dynamics of alkyl radicals is not yet understood. Our group recently started to investigate the dynamics of *tert*-butyl, *t*-C₄H₉. Earlier information on the excited states available from absorption spectroscopy⁴ and computations⁵ is summarized in Figure 1. The first band, corresponding to excitation from the X ²A₁ ground state to the A ²A₁ (3s) state, extends from 360 to 300 nm and reaches a maximum at 333 nm. The transition into the 3p band, comprising a ²A₁ and a ²E state, is centered around 253 nm. The strongest UV band corresponds to excitation to another ²A₁ state peaked at 233 nm.

We previously studied the hydrogen atom loss from optically prepared hot ground-state radicals by photofragment Doppler spectroscopy as a function of excitation energy⁶ and found, for excitation at wavelengths above 329 nm, a dissociation rate in good agreement with simple RRKM computations. However,

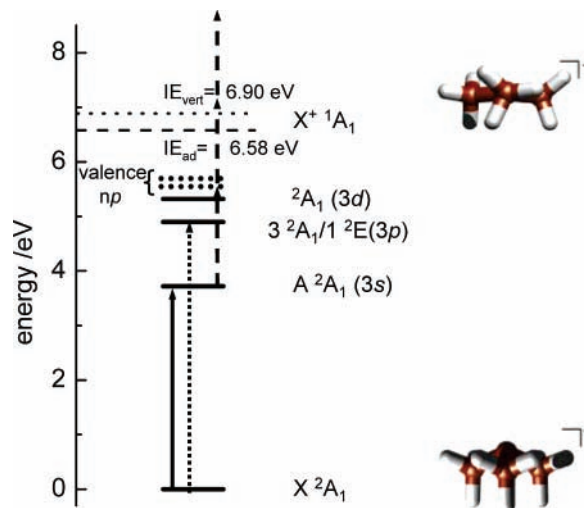


Figure 1. Relevant electronic states of the *tert*-butyl radical. The A ²A₁ state was excited between 307 and 347 nm (solid arrow), the 3p state at around 270 nm (dotted arrow). Multiphoton ionization by the 810-nm fundamental (dashed arrow) was utilized as the probe. High-lying Rydberg and valence states serve as intermediate resonances in the probe step.

when the excess energy was increased by use of wavelengths below 329 nm, a significant rate decrease by about an order of magnitude was observed. We tentatively explained this counterintuitive rate decrease by the presence of a new deactivation channel. When hot ground-state radicals are prepared by optical excitation, the interpretation of the results within statistical theories of chemical reactions relies on a conversion of

* To whom correspondence should be addressed. Phone: ++49-931/888-6360 (I.F.). Fax: ++49-931/888-6362 (I.F.). E-mail: ingo@phys-chemie.uni-wuerzburg.de (I.F.), lionel.poisson@cea.fr (L.P.).

[†] Institute of Physical Chemistry, University of Würzburg.

[‡] Institute of Organic Chemistry, University of Würzburg.

[§] Université Paris-Sud.

^{||} CEA/DSM/DRECAM/SPAM–CNRS URA 2453.

electronic energy into internal energy that is fast compared to the dissociation rate. It is generally assumed from the broad and unstructured absorption spectra that the excited states of radicals decay rapidly by internal conversion, but in most cases, including *tert*-butyl, this assumption has yet to be verified. An excellent way to study excited-state dynamics is femtosecond time-resolved spectroscopy.^{7,8} Although various frequency-domain methods^{9–11} have been applied to radical dynamics, only a few ultrafast time-resolved studies on radicals are known.^{12–14} We recently showed that the lifetime of the $2^2A'$ (3s) state of ethyl is around 20 fs and the decay thus indeed very fast,¹⁴ but little information on the underlying mechanism was obtained. In this article, we examine the excited-state dynamics of the *tert*-butyl radical by femtosecond time-resolved photoelectron spectroscopy^{15,16} at a range of pump wavelengths and outline a qualitative picture of the excited-state deactivation. In addition, we performed preliminary ab initio calculations of the electronic ground state and a number of electronically excited states in order to gain insight into the shapes and characters of the excited-state potential energy surfaces. It was our goal to obtain qualitative information on possible excited-state deactivation pathways rather than accurate electronic energies.

Experimental Section

The experiments were carried out at the Laserlab Europe femtosecond laser facility SLIC (Saclay Laser-Matter Interaction Center) at the Commissariat à l'Energie Atomique (CEA) in Saclay, France, using an experimental apparatus described elsewhere.¹⁷ A cold beam of *tert*-butyl radicals was prepared by supersonic flash pyrolysis of azo-*tert*-butane, *tert*-C₄H₉-N=N-*tert*-C₄H₉, commercially obtained from Aldrich and used without further purification. The precursor was seeded in 1.5–2.5 bar of argon and expanded through a heated SiC tube¹⁸ attached to a solenoid pulsed valve operating at 100 Hz. The heating current was adjusted for optimal conversion efficiency. Control experiments with the source turned off were performed to ensure that the observed dynamics was indeed due to pyrolytically generated radicals. After passing a 1-mm skimmer, the molecular beam reached the detection chamber, which was equipped with a time-of-flight mass spectrometer (TOF-MS) and a velocity map imaging (VMI) spectrometer used for mapping ion or electron kinetic energy distributions.¹⁹ The image analysis was performed by use of the p-Basex algorithm²⁰ implemented in a LabView program.

The femtosecond laser is a 1-kHz femtosecond Ti:Sa oscillator/amplifier chain. Tunable radiation between 260 and 350 nm for excitation (pump) was produced in a noncollinear optical parametric amplifier (NOPA), pumped by 2.5 mJ of the 810-nm fundamental (100 fs, 10-nm fwhm spectral width). The NOPA output was subsequently frequency-doubled in a KDP crystal. The central wavelengths were determined in a fiber spectrometer. The excited radicals were probed by ionization with a fraction of the residual Ti:Sa fundamental. Both laser beams were horizontally polarized. Note that, in VMI, the probe polarization has to be horizontal with respect to the imaging detector and thus cannot be rotated. No suitable waveplate was available to rotate the pump polarization. The pump–probe time delay was controlled by means of a delay line set on the pump beam and actuated by a computer-controlled stepper motor. The time intervals between two data points were not constant in a given time scan and adjusted to the slope of the decay signal. Around the zero in time, data points were taken typically every 8 fs (A^2A_1 state) or 25 fs (3p state), whereas at early and late delay times, longer intervals were chosen. The beams were

overlapped in a small angle and sent into the interaction region by a 700-mm lens. Whereas the UV beam was focused into the ionization region, the focus of the 810-nm beam lay a few millimeters away. For pump–probe contrast optimization the probe beam was attenuated by a polarizer until the one-color background signal was minimized. The probe intensity is estimated to be on the order of several 10^{11} W·cm⁻². The laser cross correlation was typically around 100 fs. In the time-delay scans, 500 shots were averaged per data point. The time-resolved photoelectron spectra reported here typically constitute an average of five such scans.

Computational Details

Because little information on the electronic states of *t*-butyl is available, aside from the geometries of the neutral²¹ and ionic ground state²² and the vertical excitation energies,⁵ we carried out ab initio calculations on the ground state and a number of excited electronic states, to describe the shapes of the potential energy surfaces as a function of the most important degrees of freedom. We emphasize that the calculations have a preliminary character and focus on a qualitative description of excited states rather than quantitatively correct energies. It was our goal to identify possible excited-state deactivation pathways, such as intersections or avoided crossings. More extensive computations of the most important degrees of freedom identified in the present work are planned.

The ground-state geometry obtained in either MP2 or DFT-(B3LYP) calculations using the Gaussian package²³ and a 6-311G** basis set served as the starting point. The energies at the optimized geometries and energies of excitation to several excited states were then computed by the CASSCF and CASPT2 methods (G3 option),^{24,25} provided by the Molcas (version 5) suite of programs.²⁶ Dunning's correlation-consistent p-VDZ basis set²⁷ was used. For a better description of Rydberg states, the basis set was augmented by two diffuse s-, p-, and d-type functions²⁸ ($\xi_s = 0.023, 0.0055$; $\xi_p = 0.021, 0.0049$; and $\xi_d = 0.015, 0.0032$) placed at the center of charge.

For the calculations, C_s symmetry was employed. Thus, both the electronic ground state and the first excited state are of A' symmetry, whereas the p Rydberg states of A_1 and E symmetry transform into two A' states and one A'' state. The active space used in the CASSCF calculations consisted of seven electrons that were distributed over 13 orbitals, nine with a' symmetry and four with a'' symmetry, resulting in a (7,13) active space. Eight a' and five a'' orbitals were kept inactive. In the computations of the potential energy as a function of nuclear coordinates, either a bond length or an angle was systematically varied in MP2 or DFT computations, and all other coordinates were optimized. Subsequently, CASSCF calculations were performed at these ground-state optimized geometries.

Results

In experiments on radicals, it is important to establish the identities of species that might contribute to the time-dependent signals. Therefore, mass spectra were recorded, as displayed in Figure 2.

With the pyrolysis source turned off and only the excitation laser (325 nm) present (top trace), no signal of the precursor azo-*tert*-butane ($m/z = 142$) was detected, and only a negligible *tert*-butyl signal was observed. The signal did not increase when the probe laser was added. When the pyrolysis source was turned on and only the excitation laser was present (center trace), a small signal of the *tert*-butyl radical at $m/z = 57$ was observed.

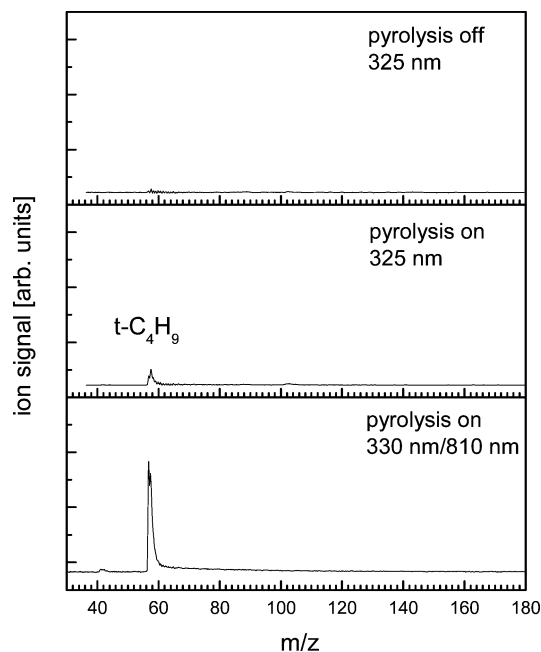


Figure 2. Typical mass spectra of azo-*tert*-butane. Only when the pyrolysis is turned on (center trace) a small *tert*-butyl signal at $m/z = 57$ appears. When the probe laser is turned on as well, the *tert*-butyl signal increases significantly (bottom trace, recorded around $t = 0$).

Note that, in the time-resolved experiments at most wavelengths, the pump laser power was kept so low that no one-color signal appeared.

When the probe laser (810 nm) was turned on in addition, the intensity of the *tert*-butyl signal increased significantly (bottom trace). The spectrum was recorded around the zero in time and at a slightly different excitation wavelength of 330 nm. All mass spectra were similar in appearance, regardless of the excitation wavelength. The second product of the pyrolysis is N_2 , which is neither excited nor ionized under our conditions. The most important channel for dissociative photoionization is loss of methane and formation of $C_3H_5^+$ (most likely 2-propenyl cation) with a thermochemical threshold of 1.85 eV above the ionization limit,²⁹ i.e., around 8.43 eV. A signal at $m/z = 41$ is indeed visible in some of the mass spectra and shows a time dependence similar to that of the *tert*-butyl peak. The small intensity of this signal indicates that the importance of dissociative photoionization, and thus higher-order processes, is negligible.

Experiments using the second harmonic of the Ti:Sa laser at 405 nm as a probe were also conducted. Because of the presence of a large probe-only background, it was not possible to extract any additional information.

a. A 2A_1 (3s) State. To elucidate the excited-state dynamics, the following three types of experiments were carried out at a number of excitation wavelengths: (a) measurements of the time-dependent ion signal, using the standard TOF-MS instrument; (b) time-resolved ion imaging; and (c) time-resolved photoelectron imaging.

As an example, photoelectron images recorded at selected delay times are presented in Figure 3. The images are dominated by a polarized contribution of p character. Because no time-dependent anisotropies were observed in any experiments, the signals obtained in the imaging studies were integrated over all angles. Thus, experiments of types (a) and (b) provided identical results. The angle-integrated electron images correspond to time-resolved photoelectron spectra. Although the time-dependent spectra of a given ion mass are indispensable in experiments

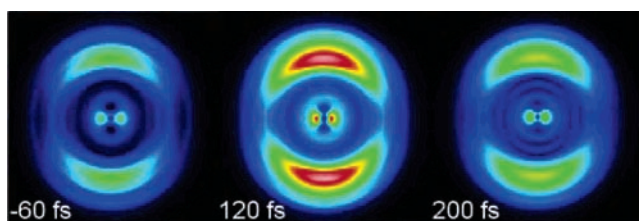


Figure 3. Photoelectron images at selected pump-probe delays, recorded at 324 nm, corresponding to excitation into the A 2A_1 (3s) state.

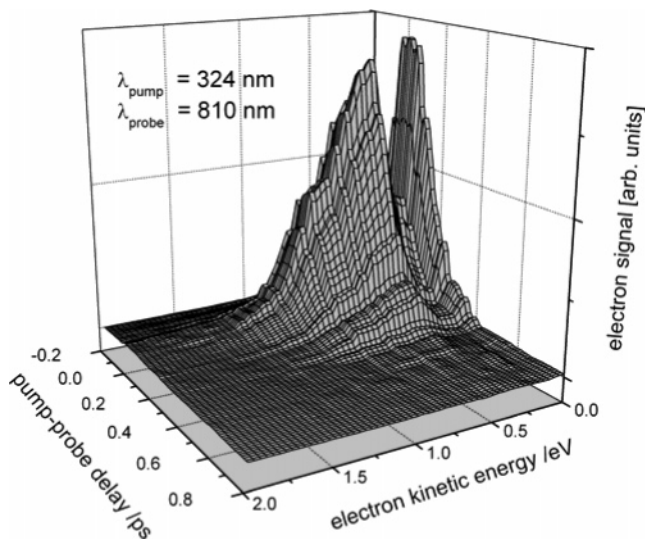


Figure 4. Time-resolved photoelectron spectrum recorded upon 324-nm excitation into the A 2A_1 state. The time dependence of the spectrum can be described by a single time constant.

on transient species because of their species selectivity, time-resolved photoelectron spectroscopy as a final-state-sensitive detection method yields additional information not available from time-dependent ion signals, as has been discussed in detail in the literature.^{16,30–34} Even though time-resolved photoelectron spectroscopy (TR-PES) is ideally suited to probe nonradiative decay processes, because of the experimental challenge only one hydrocarbon radical, allyl, C_3H_5 , has been studied before by this method,^{12,13,35} albeit at picosecond resolution only.

The photoelectron spectrum recorded upon excitation at 324 nm is depicted in Figure 4. It shows two bands, one peaking at an electron kinetic energy of 0 eV, corresponding to low-energy electrons (<100 meV), and another broad band with a maximum around 0.4 eV and a shoulder extending to higher electron kinetic energies (eKEs). The highest possible electron kinetic energy for a $[1 + 2']$ or $[1 + 3']$ process, based on an adiabatic ionization energy (IE) of 6.58 eV,³⁶ amounts to 0.30 or 1.83 eV, respectively. Thus, the band peaking at 0.4 eV is due to a $[1 + 3']$ process, whereas the low-energy signal originates either from a $[1 + 2']$ ionization or from an autoionization process following a $[1 + 3']$ excitation. Absorption of two pump photons leads to ionization at all wavelengths and will thus not yield time-dependent signals. Note that the IE of the *tert*-butyl radical is not well established and other studies place it at 6.70 eV.³⁷ The vertical IE lies between 6.90³⁶ and 6.95³⁸ eV. The signal at eKEs above 1.8 eV is very small, confirming the negligible role of higher-order processes corresponding to the absorption of more than three probe photons. No signal grows in at longer delay times.

The images were analyzed using the p-BaseX algorithm. A satisfactory fit was obtained using only the P_0 and P_2 basis

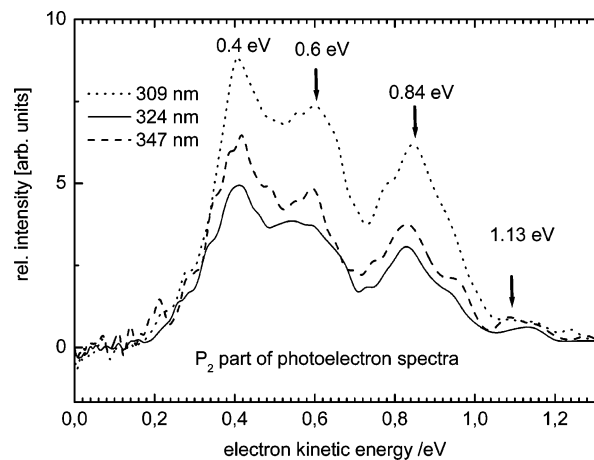


Figure 5. Polarized part of the photoelectron spectra, summed over all time delays. The spectra correspond to 347-, 324-, and 309-nm excitation. Several bands appear at the same electron kinetic energy, regardless of the excitation energy.

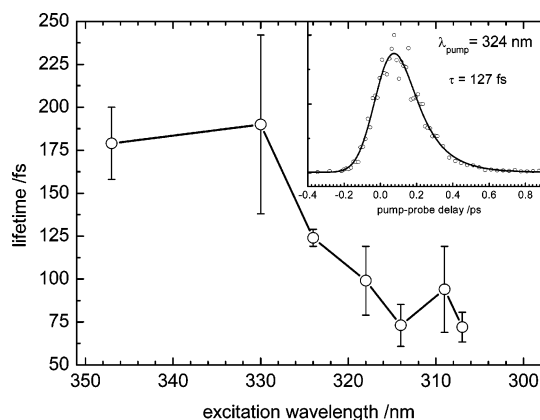


Figure 6. Measured lifetime of the A^2A_1 ($3s$) state as a function of excitation wavelength, with the 324-nm decay trace as an example.

functions. The polarized P_2 part of the broad band around 0.4 eV, summed over all delay times, is shown in Figure 5 for three selected pump wavelengths. It shows p-polarized bands at 0.4, 0.6, and 0.84 eV, as well as a rather weak band around 1.13 eV. In contrast, the low-energy band around 0 eV eKE (cf. Figure 4) does not show any polarization.

As can be seen in Figure 5, all PE spectra recorded from the 2^2A_1 state look rather similar. The position of the band maximum around 0.4 eV and the polarized bands at higher eKEs are almost independent of the excitation energy. The small signal at high eKE indicates that few transitions terminate in low-lying vibrational states of the ion. As the maximum eKE for a $[1 + 3']$ process is around 1.83 eV for a 324-nm pump, ions with a considerable amount of internal energy are formed upon ionization.

To obtain excited-state lifetimes, the intensity of the major time-dependent peak in the photoelectron spectrum was integrated, and the integral was plotted as a function of the pump-probe delay. The time dependence of all PE spectra, regardless of the excitation wavelength, could be described by a single time constant. Identical time constants were obtained upon integration of the low-energy signal. Figure 6 summarizes the decay times measured in all experiments. Each data point constitutes an average of time constants recorded in a number of time-dependent measurements of both ion and electron signals. The quality of each fit to the time-delay traces was characterized by an R^2 value. Traces with $R^2 > 0.9$ were selected for a calculation of the average. At 330 nm, only time-resolved

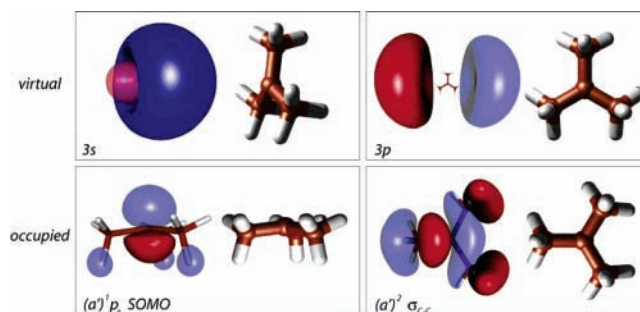


Figure 7. Relevant orbitals in the description of the electronic structure of *tert*-butyl.

TOF spectra of sufficient quality were recorded, but no TR-PE spectra. As an example, the decay curve obtained at 324 nm by integrating the $[1 + 3']$ signal between 0.21 and 0.79 eV is included as an inset in Figure 6, with the solid line being a fit to the data points that represents a convolution of the instrument response function (fwhm = 102 fs) with a monoexponential decay. The time constant obtained in this way for the population flow out of the $3s$ state was 127 fs. As can be seen, the lifetime of the A state lies around 180 fs at the red edge of the $3s$ band. Below 330 nm, it drops by more than a factor of 2 and reaches an almost constant level of around 75 fs between 307 and 320 nm.

Whereas VMI requires horizontal probe polarization, time-resolved TOF spectra were recorded with both probe polarizations. No difference was apparent in the spectra.

b. Computations. The computations yielded information on the shapes and characters of the excited electronic states, as well as on the possible presence of curve crossings. The ground-state geometry obtained from MP2 computations is similar to that obtained in earlier work.²¹ Only a slightly larger C–C bond length of 1.508 Å as compared to 1.493 Å was found. In all DFT and most MP2 calculations, the $\langle \hat{S}^2 \rangle$ eigenvalues were around 0.75; only MP2 calculations at extended C–C bond lengths (> 2.1 Å) yielded somewhat larger values. The characters of the molecular orbitals (MOs) most important for the present study also agree with results of earlier work.⁵ MOs averaged over all states are depicted in Figure 7. Note that the scales of the molecule are different for occupied and virtual orbitals, but identical for both virtual orbitals. All low-lying electronic states are dominated ($> 90\%$) by a single electron configuration in the CASSCF computation at the ground-state equilibrium geometry. As can be seen, the singly occupied molecular orbital (SOMO, lower left) can be described as a p orbital on the carbon radical center. The A^2A_1 state corresponds to excitation of the electron from the SOMO into the first virtual orbital (upper left), a diffuse orbital with Rydberg s character. The 3^2A_1 and 1^2E states are adequately described as a $3p$ Rydberg state. One of the corresponding orbitals is depicted on the upper right side of Figure 7.

Vertical excitation energies were computed at the CASSCF and CAS-PT2 levels of theory. The results are summarized in Table 1 and compared to the experimental values as well as earlier CI calculations by Lengsfeld et al.⁵ Whereas the CASSCF results underestimate the excitation energies significantly, the CAS-PT2 results are consistently higher than the experimental values. In agreement with Lengsfeld et al., we find the lowest excited valence state of $2E$ symmetry to be at rather high energies, with computed values above the experimental ionization energy. At the ground-state equilibrium geometry, this corresponds to the excitation of an electron from a σ -bonding molecular orbital (lower right in Figure 7) to the

TABLE 1: Vertical Excitation Energies (eV) at the MP2 Ground-State Equilibrium Geometry

electronic state	CASSCF	CAS-PT2	ref 5	experiment ^d
3s	3.25/3.63 ^a	4.36	4.17	3.75
3p (² A ₁)	3.76/4.04 ^a	5.10	4.79	4.86 ^b
3p (² E)	3.90	5.17	4.98	4.86 ^b
3d (² A)	4.41	5.69	5.35	5.17
3d (² A)	4.46	5.85	5.35	5.32
² E (valence)	7.23	6.95	7.73	

^a Excitation energies obtained after optimization of angle β ; see Figure 9. ^b The two components of the 3p state were not separated in the experiment.

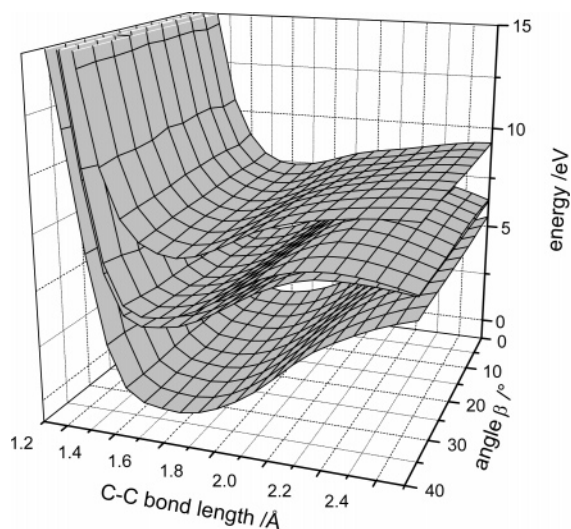


Figure 8. CASSCF potential energy surfaces of the electronic ground state, the first two excited states, and the first excited valence state as a function of the C–C bond length (corresponding to the symmetric stretch motion) and the carbon framework angle β .

singly occupied orbital on the radical center and constitutes the $8^2A'$ state in C_s symmetry. The lowest-energy A'' states are 3p and 3d Rydberg states. They were computed to behave similarly to the corresponding A' states and will not be discussed further.

Because the electronic character of a state can be different at geometries far from the ground-state equilibrium geometry, we computed the energies of all electronic states of A' symmetry up to the first valence state as a function of several important nuclear coordinates. Figure 8 shows the potential energy dependence computed at the CASSCF level along the symmetric C–C stretching motion and the carbon framework angle β , defined in the inset of Figure 9, for the ground state as well as the A^2A_1 , 3^2A_1 , and first excited valence states. No avoided crossings or intersections between surfaces are visible. The electronic character of the X^2A_1 and A^2A_1 state is preserved over both coordinates.

Whereas r_{C-C} changes little upon excitation, a significant geometry change is found for the angle β (defined as $180^\circ -$ dihedral angle) of the carbon framework. Therefore, we carried out a more detailed investigation with additional data points. Figure 9 represents a cut through Figure 8 at $r_{C-C} = 1.508 \text{ \AA}$, the ground-state equilibrium distance. As can be seen, the A^2A_1 state has an ion-like planar carbon framework, as expected for a Rydberg state. The potential of the 3^2A_1 (3p) state along the angular coordinate is similar. Note that the MP2 computations yield a dihedral angle of 154.7° for the ground state, whereas the CASSCF calculation yields 148° and thus a more pyramidal geometry. The energy difference of roughly 0.4 eV between the vertical and adiabatic excitation energies leads to

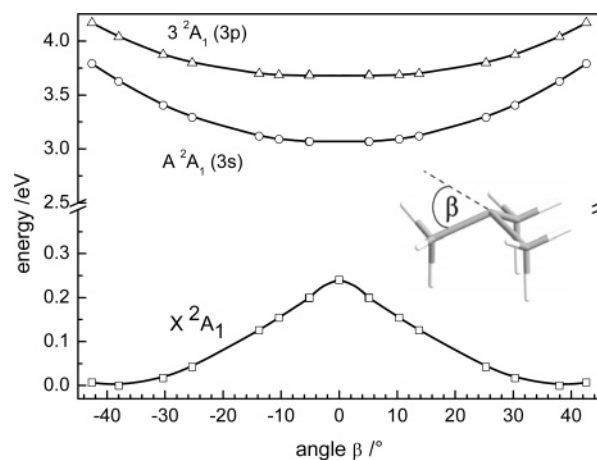


Figure 9. CASSCF potential energies of the electronic ground state and the first two excited states as a function of the carbon framework angle β defined in the inset.

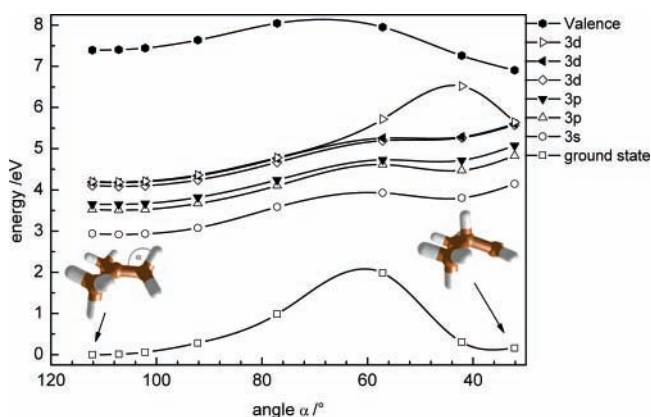


Figure 10. Potential energy as a function of the angle α , corresponding to the coordinate for 1,2-H-atom shift, for the lowest states of A' symmetry.

an out-of-plane bending motion after electronic excitation and explains the rather broad bands in the absorption spectrum.⁴

We also considered isomerization as a possible reaction pathway, proceeding via a 1,2-H-atom shift from *tert*-butyl to the primary isobutyl radical. The computed potentials along this coordinate corresponding to a change of the angle α are depicted in Figure 10. MP2 computations of the ground-state potential with more data points yielded a barrier of 2.08 eV to isomerization (see Supporting Information). For comparison, in ethyl³⁹ the barrier to H-atom shift in the electronic ground state was computed to be around 1.76 eV. The isobutyl radical was calculated to lie 0.2 eV (19 kJ/mol) above *tert*-butyl, in good agreement with the thermochemical value of 22 kJ/mol. In the 3s and 3p states, the energy difference between the two isomers is higher (around 0.89 eV in the 3s state, with a 1.01 eV barrier), in agreement with the significant red shift of the first electronic absorption band in tertiary alkyl radicals as compared to primary radicals.⁴ No photochemical funnel from the excited state to the electronic ground state of either *tert*-butyl or isobutyl was found. Most likely, the isomerization coordinate is not important for the excited-state deactivation of *tert*-butyl.

Another coordinate of interest is the asymmetric C–C stretch motion, corresponding to direct rupture of a carbon–carbon bond and formation of dimethylcarbene and a methyl radical. When only one C–C bond is stretched, the lowest valence state correlates to the singlet ground state of the carbene. The valence-state energy is therefore expected to decrease significantly along this coordinate. A direct cleavage of the C–C bond is not

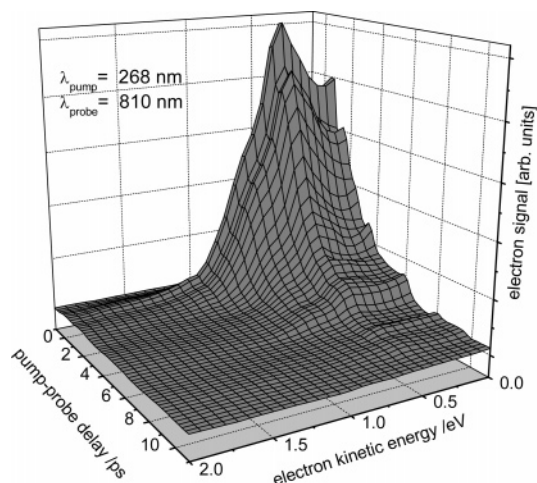


Figure 11. Time-resolved PE spectra recorded upon 268-nm excitation into the 3p state. Again, the time dependence can be described by a single time constant, which is in the picosecond regime.

feasible upon 3s excitation because it requires $\Delta_R H(0\text{ K}) = +395\text{ kJ/mol}$ (4.1 eV), in agreement with earlier work.⁴⁰ However, the valence state and the 3s state cross at extended C–C bond lengths, indicating significant nonadiabatic interactions between the two states. Preliminary computations thus suggest that motion along the asymmetric C–C stretch is important for the photophysics of *tert*-butyl. We plan to address this question by carrying out multireference CI computations.

We also examined the potential along one C–H stretch, corresponding to C–H bond rupture, and found the $2\ ^2A_1$ state to be bound along the C–H bond. Although the electronic character of the ground state did not change, interactions between the 3s and the valence state were identified. Again, a conclusive answer concerning the role of this degree of freedom requires more extensive computations.

Overall, the excited-state energies are off by approximately 0.5 eV. However, we believe that the computations represent the qualitative features correctly and can thus aid in a discussion of the experimental results.

c. $3\ ^2A_1/1\ ^2E$ (3p) State. The PE spectrum recorded from the 3p state upon excitation at 268 nm is displayed in Figure 11. The p-Basex analysis yields only a weak polarization. Note that the 3p state has two components, 2A_1 and 2E , that cannot not be separated in the absorption spectrum. The spectrum is dominated by $[1 + 2']$ ionization, but a small signal is present at kinetic energies higher than the maximum available energy of 1.1 eV. This signal might be due to either higher-order processes or pump–probe processes originating from hot bands. The spectrum obtained upon 274-nm excitation looks very similar. Both wavelengths, 268 and 274 nm, correspond to excitation on the red edge of the 3p band.

From FC considerations, one again expects intense transitions to low-lying vibrational states of the ion, because the geometry of the Rydberg state will resemble that of the ion. However, the PE spectrum shown in Figure 11 peaks at an eKE of 0.44 eV, corresponding to ions with a considerable internal energy of 0.66 eV. As in the spectra from the 3s state, the ionization step thus terminates in excited vibrational states of the ion. The signal decays to zero at long delay times, and no band grows in over the time. Figure 12 shows the time-dependent ion signal obtained at 268 nm that can be described by a single decay constant of 2 ps. A biexponential fit using an additional sub-100-fs decay time resulted in only a marginally better R^2 value and is therefore not justified by the experimental data. A similar

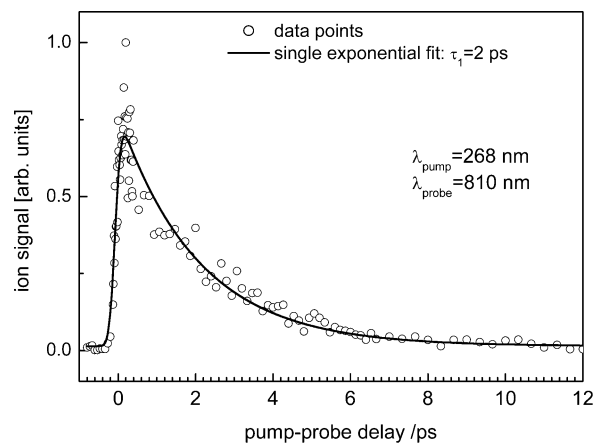


Figure 12. Time-dependent ion signal upon 268-nm excitation into the 3p state.

time constant was measured upon 274-nm excitation, albeit at an inferior signal-to-noise ratio.

Discussion

The geometry of *tert*-butyl changes from the slightly pyramidal C_{3v} geometry of the neutral ground state to a planar carbon framework upon ionization. The minimum-energy conformer of the ion has no symmetry because of the hindered methyl rotors, but the C_{3h} conformer is only slightly higher in energy.^{22,41} Thus, the potential energy surface is rather flat, as is usually the case when a 6-fold rotational barrier is present. Because of this geometry change, the vertical and adiabatic IEs obtained by conventional PES differ by 0.2–0.3 eV, and the PE spectra³⁶ show activity in the bending mode ($460 \pm 30\text{ cm}^{-1}$) and the symmetric C–C stretch ($760 \pm 30\text{ cm}^{-1}$). As calculated, the low-lying excited electronic states have Rydberg character, and their geometries resemble the ionic geometry. This is confirmed by the electron images shown in Figure 3, which are dominated by a p-polarized contribution and can be described as originating from a state with dominant s character. Because a 324-nm pump will deposit roughly 0.4 eV of vibrational energy in the $2\ ^2A_1$ (3s) state, mostly in the out-of-plane bending mode, it is surprising that more than 1 eV of internal energy is deposited in the ion, because a vertical transition is expected between states of similar geometries. Note that a probe laser intensity of some 10^{11} W cm^{-2} is too small to affect the appearance of the PE spectra, because the ponderomotive shift,^{42–44} U_p , will be on the order of only 10–20 meV under our conditions.

A likely explanation for the appearance of the photoelectron spectra as well as the independence of the excitation energy is an enhancement by accidental intermediate resonances, as has been discussed in relation to $[1 + 2']$ femtosecond time-resolved photoelectron spectra on pyrazine⁴⁵ and pyridine.⁴⁶ In a $[1 + 3']$ experiment from the 3s state, the probe step might be enhanced by an *np* Rydberg state or by a two-photon *ms* or *nd* resonance close to or above the ionization limit. As such states are also ion-like, they cannot fully explain the broad PE spectra. We therefore believe that the PE spectra are rather influenced by an intermediate high-lying valence state and reflect the structure of the resonances of this accidental intermediate in addition to the 3s state. Note that frequency-domain photoelectron spectra of CH_3I ^{47–49} and other haloalkanes,^{50,51} recorded via one-color multiphoton absorption, also carry the signature of intermediate states. The same arguments hold for the spectrum

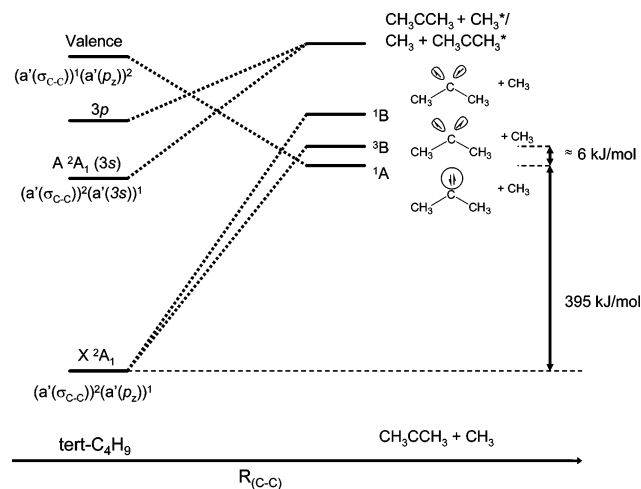


Figure 13. Correlation diagram, connecting several states of *t*-C₄H₉ with the H₃CCCH₃ + CH₃ product channel. The valence state is expected to cross both the 3s state and the ground state.

recorded at 268 nm (cf. Figure 11), because absorption of one 810-nm probe photon excites *tert*-butyl to an unassigned high-lying state around 200 nm (6.20 eV). Electrons produced by autoionization will generally appear close to zero kinetic energy and are therefore not expected to contribute to the bands in the PE spectrum.

No signal growing in from a lower electronic state was identified in our time-resolved PE spectra. The fast rate suggests decay through a conical intersection. Many possible excited-state deactivation channels, such as excited-state isomerization or the symmetric C–C stretch motion, can be ruled out by our calculations as described above. However, the computations indicate the possibility of avoided curve crossings or photochemical funnels along the asymmetric C–C stretching motion that leads to the dimethylcarbene + methyl product channel. Their presence can be qualitatively understood when we consider the correlation of the *tert*-butyl electronic states with the product states, as shown in Figure 13: When the electronic ground state dissociates, the electrons in the σ_{C-C} MO will be distributed between the two fragments, and the carbene product is formed either in its ³B triplet state or in the ¹B open-shell singlet. The valence state, on the other hand, has the orbital occupancy $[a'(\sigma_{C-C})^1][a'(p_z)^2]$, so when one C–C bond is cleaved, the electron in the σ_{C-C} MO becomes an electron in the SOMO on the methyl radical. The $(p_z)^2$ electrons remains at the carbon; thus, the valence state correlates to the ¹A closed-shell singlet state of dimethylcarbene. Several theoretical studies have assigned the ¹A state as the ground state and place the triplet above it, although by only a small margin.^{52–54} The 3s state, on the other hand, correlates to an excited electronic state of one the products, presumably the 3s state of CH₃.

As a consequence of this state-to-state correlation, the valence state will cross the 3p, 3s, and ground states, presumably at an extended C–C bond length. Motion along the asymmetric C–C stretching coordinate could thus provide an efficient channel for excited-state deactivation. Note that direct cleavage of the C–C bond requires 4.1 eV and is not possible upon 3s excitation. The energy range in which the state crossing is relevant for the photophysics of *tert*-butyl depends on the shape of the multidimensional potential energy surface, i.e., factors such as deformation along other degrees of freedom. In further computations, we will investigate the crossing region in more detail. Note that all alkyl radicals have similar excited-state configurations. The energy of a valence state with $(\sigma_{C-C})^1(p_z)^2$ orbital occupancy will decrease along a coordinate leading to

C–C bond dissociation and cross low-lying Rydberg states. Interactions between the valence and ground states will depend on the carbene ground-state multiplicity and singlet–triplet gap. To summarize, we suggest this crossing with a valence state to be an important deactivation pathway for the Rydberg states of alkyl radicals. This was initially suggested by Herzberg as an explanation for the diffuse appearance of the electronic spectrum of the methyl B ²A₁' state.⁵⁵

The time-resolved PE spectra (cf. Figure 4) do not provide any information on the final state of the nonradiative decay. Therefore, we consider the orbital correlations in photoionization for the valence state, following the arguments outlined by Stolow and co-workers.^{16,34} Both the X ²A₁ ground state and the A ²A₁ (3s) state can be ionized to the ground state of the cation by ejecting the unpaired electron. In contrast, removal of one electron from the $a'(p_z)$ HOMO of the valence state will form an excited electronic state of the cation. Consequently, if an excited state with valence character were formed nonradiatively, its ionization cross section to the cationic ground state would be small, and our experiments might miss its contribution to the photophysics. In principle, a state with valence character could be efficiently ionized to an excited cationic state, but because the first excited electronic state of *t*-C₄H₉⁺ lies at 11.64 eV,³⁶ such an experiment will be challenging.

Two electronic states that cannot be separately excited contribute to the 3p band, ³ ²A₁ and ¹ ²E. Transitions into the ²E components are expected to be weak because, in the limit of planar geometry, corresponding to the X ²A₂'' ↔ ²E' transition in methyl, the transition will be forbidden.⁵⁶ The measured lifetime of the 3p state is surprisingly long, given the diffuse and unstructured absorption spectrum. We reproduced the shape of the 3p band as reported by Wendt and Hunziker⁴ in MPI experiments with a tunable nanosecond laser without identifying any vibronic structure. The diffuse nature of the band might be due to a fast relaxation process that we cannot resolve, but it is also possible that the reason for the lack of vibronic structure is a very high density of states. The time constant of 2 ps for population flow out of the 3p state corresponds to internal conversion either to the ² ²A₁ (3s) state or to the valence state, which also crosses the 3p state (cf. Figure 13). In a second step, the radical could deactivate rapidly to the electronic ground state with a time constant that cannot be resolved in our experiments. Again, no photoelectron signal would be visible at long decay times. The amount of vibrational energy present in the ground-state radical after excitation at 268 nm (4.63 eV) would be too high to allow efficient ionization to low-lying vibrational states of the ion.

In our earlier photofragmentation study on the channel leading to C₄H₈ (2-methyl propene) + H ($\Delta_R H^\circ = 152 \pm 3$ kJ/mol), we observed a H-atom loss occurring on the nanosecond time scale.⁶ The femtosecond time-resolved data presented above support the picture of a rapid excited-state deactivation, forming hot ground-state *tert*-butyl radicals that lose H atoms in the rate-determining step on a nanosecond time scale. However, in the nanosecond experiments,⁶ a counterintuitive drop in the dissociation rate was observed at excitation energies above 3.75 eV ($\lambda_{\text{pump}} < 330$ nm), corresponding to the blue part of the 3s absorption and the 3p band. In this earlier study, we suggested that coupling to an optically dark electronic state, such as the valence state discussed above, might play a role in the excited-state dynamics. Interestingly, the A ²A₁ lifetimes depicted in Figure 6 show a drop between 329 and 320 nm, i.e., in the same energy region where the rates in the photofragmentation experiments change. Future computations will show whether a

curve crossing or a photochemical funnel along the asymmetric C–C stretch motion becomes accessible in this energy region. Given the short excited-state lifetimes, the decrease in the dissociation rate observed in the nanosecond experiments seems to be due to effects taking place on the ground-state potential energy surface. In one possible scenario, the radical could return to the ground-state surface far from the equilibrium geometry. Bottlenecks on the potential energy surface might hamper the rapid redistribution of vibrational energy and limit the applicability of statistical theories. An alternative explanation was recently provided for ethyl, C₂H₅: In earlier experiments, rates for H-atom loss were found to be even several orders of magnitude lower than expected from a simple RRKM model.⁵⁷ A classical trajectory study of ethyl dissociation⁵⁸ identified quasiperiodic orbits that lead to population trapping. Consequently, the surprisingly slow photodissociation of ethyl was explained by an incomplete randomization of energy. It remains to be shown whether similar effects also play a role in the photofragmentation of the *tert*-butyl radical.

Conclusion

We investigated the excited-state dynamics of isolated *tert*-butyl radicals in a molecular beam by femtosecond time-resolved photoionization, photoelectron spectroscopy, and both ion and electron imaging. Electronic structure calculations yielded insight into the shapes and characters of the excited-state potential energy surfaces. *tert*-Butyl was generated from azo-*tert*-butane by flash pyrolysis. The radicals were optically excited into the A ²A₁ (3s) state between 347 and 307 nm and the 3p band at 274 and 268 nm. Multiphoton ionization by 810-nm radiation served as the probe step. The Rydberg character of the excited states was confirmed by ab initio computations and for the 3s state by the polarization of the photoelectron images. At all wavelengths, the photoelectron spectra are broad and peaked at low electron kinetic energies. They are influenced by accidental intermediate resonances in the probe step, either high-lying Rydberg or valence states. The excited-state deactivation can be described in all cases by a single exponential decay time constant, but no signal growing in from the final electronic state was observed. We measured time constants between 180 and 75 fs for the population flow out of the A ²A₁ state. For the 3p state, a lifetime of 2 ps was measured, more than a factor of 10 longer than for the lower-lying 3s state. The 3p state seems to decay in a two- or even multistep process via the valence state and/or the lower-lying 3s state. The computed values for electronic excitation energies are off by roughly 0.5 eV, but the shapes of the excited-state potential energy surfaces are described correctly. In agreement with expectations, the carbon-atom framework becomes planar in the Rydberg excited states, which explains the broad absorption spectra. The barriers to isomerization to the isobutyl radical were computed to be 2.07 eV in the ground state and 1.01 eV in the A ²A₁ state. The existence of intersections or avoided curve crossings along the coordinate leading to excited-state isomerization as well as along the symmetric C–C stretching motion can thus be ruled out. The most relevant degree of freedom is probably the asymmetric C–C stretching motion, corresponding to dissociation into dimethylcarbene and methyl. The dissociation energy, *D_e*, was calculated to be 395 kJ/mol. Qualitative considerations indicate a crossing between the A ²A₁ (3s) state and the lowest valence state, but also a crossing between the valence state and the ground state along the asymmetric C–C stretching motion. This picture is supported by preliminary ab initio calculations. More accurate calculations are required to confirm whether this crossing is responsible for the fast excited-state deactivation.

Acknowledgment. This work was supported by the Deutsche Forschungsgemeinschaft under Contract Fi 575/3-3 and by the Graduiertenkolleg GRK 1221. Financial support from the Access to Research Infrastructures activity in the Sixth Framework Programme of the EU (Contract RII3-CT-2003-506350, Laserlab Europe) for conducting the research, from the German/French binational PROCOPE program, and from the BFHZ (Bayrisch-Französisches Hochschulzentrum) is gratefully acknowledged. The authors thank B. Soep for fruitful discussions and O. Gobert, M. Perdrix, F. Lepetit, J. F. Hergott, and D. Garzella for developing, maintaining, and running the femtosecond laser facility PLFA (Plateforme Laser Femtoseconde Accordable) of the CEA, DSM/DRECAM.

Supporting Information Available: Full citations for refs 3, 23, and 26; MP2 ground-state geometry; ground-state potential energy curves along the isomerization coordinate and the C–C bond cleavage coordinate (asymmetric C–C stretch); and Cartesian coordinates of all points discussed in this article. This material is available free of charge via the Internet at <http://pubs.acs.org>.

References and Notes

- (1) Warnatz, J. In *Combustion Chemistry*; Gardiner, W. C. J., Ed.; Springer: New York, 1984.
- (2) Mahaffy, P. R. *Science* **2005**, *308*, 969.
- (3) Waite, J. H., Jr. et al. *Science* **2005**, *308*, 982.
- (4) Wendt, H. R.; Hunziker, H. E. *J. Chem. Phys.* **1984**, *81*, 717.
- (5) Lengsfeld, B. H., III; Siegbahn, P. E. M.; Liu, B. *J. Chem. Phys.* **1984**, *81*, 710.
- (6) Zierhut, M.; Roth, W.; Fischer, I. *J. Phys. Chem. A* **2004**, *108*, 8125.
- (7) Zewail, A. H. *J. Phys. Chem.* **1996**, *100*, 12701.
- (8) Zewail, A. H. *Angew. Chem., Int. Ed.* **2000**, *39*, 2586.
- (9) Butler, L. J.; Neumark, D. M. *J. Phys. Chem.* **1996**, *100*, 12801.
- (10) Continetti, R. E. *Annu. Rev. Phys. Chem.* **2001**, *52*, 165.
- (11) Fischer, I.; Chen, P. *J. Phys. Chem. A* **2002**, *106*, 4291.
- (12) Schultz, T.; Fischer, I. *J. Chem. Phys.* **1997**, *107*, 8197.
- (13) Schultz, T.; Clarke, J. S.; Deyler, H.-J.; Gilbert, T.; Fischer, I. *Faraday Discuss.* **2000**, *115*, 17.
- (14) Zierhut, M.; Noller, B.; Schultz, T.; Fischer, I. *J. Chem. Phys.* **2005**, *122*, 094302.
- (15) Neumark, D. M. *Annu. Rev. Phys. Chem.* **2001**, *52*, 255.
- (16) Stolow, A. *Annu. Rev. Phys. Chem.* **2003**, *54*, 89.
- (17) Poisson, L.; Raffael, K. D.; Soep, B.; Mestdagh, J.-M.; Buntinx, G. *J. Am. Chem. Soc.* **2006**, *128*, 3169.
- (18) Kohn, D. W.; Clauberg, H.; Chen, P. *Rev. Sci. Instrum.* **1992**, *63*, 4003.
- (19) Eppink, A. T. J. B.; Parker, D. H. *Rev. Sci. Instrum.* **1997**, *68*, 3477.
- (20) Garcia, G.; Nahon, L.; Powis, I. *Rev. Sci. Instrum.* **2004**, *75*, 4989.
- (21) Pacansky, J.; Koch, W.; Miller, M. D. *J. Am. Chem. Soc.* **1991**, *113*, 317.
- (22) East, A. L. L. *J. Chem. Phys.* **1997**, *107*, 3914.
- (23) Frisch, M. J. et al. *Gaussian 03*, revision B.04; Gaussian Inc.: Pittsburgh, PA, 2003.
- (24) Andersson, K.; Malmqvist, P.-A.; Roos, B. O. *J. Chem. Phys.* **1992**, *96*, 1218.
- (25) Andersson, K.; Malmqvist, P.-A.; Roos, B. O.; Sadlej, A. J.; Wolinski, K. *J. Phys. Chem.* **1990**, *94*, 5483.
- (26) Andersson, K. et al. *Molcas*, version 5; Lund University: Lund, Sweden, 2000.
- (27) Dunning, T. H., Jr. *J. Chem. Phys.* **1989**, *90*, 1007.
- (28) Poirier, R.; Kari, R.; Csizmadia, I. G. *Handbook of Gaussian Basis Sets*; Elsevier: New York, 1985.
- (29) Aubry, C.; Holmes, J. L. *J. Phys. Chem. A* **1998**, *102*, 6441.
- (30) Stolow, A.; Bragg, A. E.; Neumark, D. M. *Chem. Rev.* **2004**, *104*, 1719.
- (31) Pallix, J. B.; Colson, S. D. *Chem. Phys. Lett.* **1985**, *119*, 38.
- (32) Blanchet, V.; Zgierski, M. Z.; Stolow, A. *J. Chem. Phys.* **2001**, *114*, 1194.
- (33) Schmitt, M.; Lochbrunner, S.; Shaffer, J. P.; Larsen, J. J.; Zgierski, M. Z.; Stolow, A. *J. Chem. Phys.* **2001**, *114*, 1206.
- (34) Blanchet, V.; Lochbrunner, S.; Schmitt, M.; Shaffer, J. P.; Larsen, J. J.; Zgierski, M. Z.; Seideman, T.; Stolow, A. *Faraday Discuss.* **2000**, *115*, 33.

- (35) Schultz, T.; Fischer, I. *J. Chem. Phys.* **1998**, *109*, 5812.
- (36) Dyke, J. M.; Jonathan, N.; Lee, E.; Morris, A.; Winter, M. *Phys. Scr.* **1977**, *16*, 197.
- (37) Houle, F. A.; Beauchamp, J. L. *J. Am. Chem. Soc.* **1979**, *101*, 4067.
- (38) Koenig, T.; Balle, T.; Snell, W. *J. Am. Chem. Soc.* **1975**, *97*, 662.
- (39) Mebel, A. M.; Morokuma, K.; Lin, M. C. *J. Chem. Phys.* **1995**, *103*, 3440.
- (40) Ford, F.; Yuzawa, T.; Platz, M. S.; Matzinger, S.; Fülischer, M. *J. Am. Chem. Soc.* **1998**, *120*, 4430.
- (41) Sieber, S.; Buzek, P.; Schleyer, P. v. R.; Koch, W.; Carneiro, J. W. d. M. *J. Am. Chem. Soc.* **1993**, *115*, 259.
- (42) Bucksbaum, P. H.; Freeman, R. R.; Bashkansky, M.; McIlrath, T. *J. J. Opt. Soc. Am.* **1987**, *B 4*, 760.
- (43) Freeman, R. R.; Bucksbaum, P. H.; McIlrath, T. *J. IEEE J. Quantum Electron.* **1988**, *24*, 1461.
- (44) Zavrijev, A.; Fischer, I.; Villeneuve, D. M.; Stolow, A. *Chem. Phys. Lett.* **1995**, *234*, 281.
- (45) Song, J.-K.; Tsubouchi, M.; Suzuki, T. *J. Chem. Phys.* **2001**, *115*, 8810.
- (46) Tsubouchi, M.; Suzuki, T. *J. Phys. Chem. A* **2003**, *107*, 10897.
- (47) Strobel, A.; Lochschmidt, A.; Fischer, I.; Niedner-Schatteburg, G.; Bondybey, V. E. *J. Chem. Phys.* **1993**, *99*, 733.
- (48) Strobel, A.; Fischer, I.; Lochschmidt, A.; Müller-Dethlefs, K.; Bondybey, V. E. *J. Phys. Chem.* **1994**, *98*, 2024.
- (49) Schultz, T.; Fischer, I. *J. Phys. Chem. A* **1997**, *101*, 5031.
- (50) Knoblauch, N.; Strobel, A.; Fischer, I.; Bondybey, V. E. *J. Chem. Phys.* **1995**, *103*, 5417.
- (51) Macleod, N. A.; Wang, S.; Hennessy, J.; Ridley, T.; Lawley, K. P.; Donovan, R. J. *J. Chem. Soc., Faraday Trans.* **1998**, *94*, 2689.
- (52) Matzinger, S.; Fülischer, M. *J. Phys. Chem.* **1995**, *99*, 10747.
- (53) Demel, O.; Pittner, J.; Carsky, P.; Hubac, I. *J. Phys. Chem. A* **2004**, *108*, 3125.
- (54) Richards, C. A.; Kim, S.-J.; Yamaguchi, Y.; Schaefer, H. F., III. *J. Am. Chem. Soc.* **1995**, *117*, 10104.
- (55) Herzberg, G. *Electronic Spectra and Electronic Structure of Polyatomic Molecules*; Krieger: Melbourne, FL, 1991.
- (56) Hollas, J. M. *High-Resolution Molecular Spectroscopy*, 2nd ed.; Wiley: New York, 1998.
- (57) Gilbert, T.; Grebner, T. L.; Fischer, I.; Chen, P. *J. Chem. Phys.* **1999**, *110*, 5485.
- (58) Bach, A.; Hostettler, J. M.; Chen, P. *J. Chem. Phys.* **2005**, *123*, 021101.